nature communications

Article

https://doi.org/10.1038/s41467-026-68957-5

Bio-based oxalic acid production in *Issatchenkia orientalis* enables sustainable rare earth recovery

Received: 18 May 2025

Accepted: 21 January 2026

Published online: 30 January 2026

Check for updates

Jingxia Lu[1,2], Wenjun Guo[3,4], Ziye Dong[5], Sarang S. Bhagwat[3,4], Shih-I Tan[1], Zhixin Zhu[1,2], Andrew Johnson[6], Jeremy S. Guest[3,4,7], Rick Honaker[6], Dan M. Park[5], Yongqin Jiao[5] & Huimin Zhao[1,2,3,8]

The growing demand for rare earth elements (REEs) in clean energy and high-tech industries underscores the need for sustainable recovery methods and a reliable supply of processing chemicals. Here, we establish a microbial platform using the acid-tolerant yeast *Issatchenkia orientalis* SD108 to produce bio-oxalic acid for REE recovery. By introducing an oxaloacetate cleavage pathway and applying metabolic engineering, the engineered strain produces 39.53 $g{\cdot}L^{-1}$ oxalic acid at pH 4.0 in fed-batch fermentation. The crude fermentation broth, used without purification, efficiently precipitates over 99% neodymium (Nd), 99% dysprosium (Dy), and 98% lanthanum (La) from individual REE chloride solutions. Recovery from a low-grade ore leachate achieves over 99% total recovery. X-ray diffraction (XRD) and Fourier transform infrared spectroscopy (FTIR) confirm that REE oxalates precipitated with bio-oxalic acid closely resemble those obtained using commercial oxalic acid. Techno-economic analysis (TEA) and life cycle assessment (LCA) further demonstrate that bio-oxalic acid can be produced at a competitive price of $\$1.79{\cdot}kg^{-1}$ while reducing carbon intensity (CI) by 112% to 63.5% with and without electricity displacement, respectively, relative to the fossil-based benchmark. These results highlight bio-oxalic acid as a green, economically viable alternative to synthetic oxalate for sustainable REE recovery.

Rare earth elements (REEs) comprise 17 chemical elements including 15 lanthanides, yttrium (Y), and scandium (Sc), and play a crucial role in the development of civilization and human life[1]. For example, some REEs, such as neodymium (Nd), praseodymium (Pr), terbium (Tb), and dysprosium (Dy) are used to produce magnets that are important to electronic vehicles (EVs) and wind turbines[2]. The global demand for REEs is projected to grow by 41% in 2030, highlighting the need for reliable sources of REEs[2]. This unmet need has recently driven exploration efforts, the development of mining and processing facilities for REE-containing minerals, and the pursuit of more sustainable strategies for REE recovery[3]. Oxalic acid ($C_2H_2O_4$, OA) is widely used in the purification of REEs owing to its strong affinity for REE^{3+} ions and its

[1]The Grainger College of Engineering, Department of Chemical and Biomolecular Engineering, University of Illinois Urbana-Champaign, Urbana, IL, USA. [2]Carl R. Woese Institute for Genomic Biology, University of Illinois Urbana-Champaign, Urbana, IL, USA. [3]DOE Center for Advanced Bioenergy and Bioproducts Innovation, University of Illinois Urbana-Champaign, Urbana, IL, USA. [4]The Grainger College of Engineering, Department of Civil and Environmental Engineering, University of Illinois Urbana-Champaign, Urbana, IL, USA. [5]Physical and Life Sciences Directorate, Lawrence Livermore National Laboratory, Livermore, CA, USA. [6]Department of Mining Engineering, University of Kentucky, Lexington, KY, USA. [7]Institute for Sustainability, Energy, and Environment (iSEE), University of Illinois Urbana-Champaign, Urbana, IL, USA. [8]NSF Molecule Maker Lab Institute, University of Illinois Urbana-Champaign, Urbana, IL, USA. e-mail: zhao5@illinois.edu

ability to selectively precipitate REEs from solution under low pH conditions[4,5]. This chemistry enables efficient REE recovery with minimal co-precipitation of non-REE metals, even in the presence of high levels of impurities such as Fe^{3+} and Al^{3+}[6]. Oxalic acid precipitation is employed at various stages in REE processing: it can upgrade total REE concentrations in mixed REE leachate solutions[6], and is used to precipitate individually separated REEs following solvent extraction during REO (rare earth oxide) production[7].

Oxalic acid is primarily used as a cleaning and bleaching agent with additional applications in metal surface treatment, chemical synthesis and agricultural formulations. The oxalic acid market is experiencing substantial growth, driven by its increasing application in the wood and metal industries[8]. Additionally, rising demand from the pharmaceutical sector is contributing significantly to the expansion of the global oxalic acid market. It has been reported that the global oxalic acid market size reached USD 1.57 billion in 2024, and was projected to reach USD 2.35 billion by the end of 2034, expanding at a compound annual growth rate (CAGR) of 4.12% during the forecast period[9]. Currently, oxalic acid is primarily produced through chemical routes, such as the oxidation of propylene or ethylene glycol using strong acids, or through carbon monoxide-based dialkyl oxalate synthesis. Although these methods provide high yields, they depend on fossil-derived feedstocks and involve hazardous reagents, high energy consumption, and costly catalysts[10]. Environmental concerns and complex downstream processing further limit their sustainability. The biological production of oxalic acid using engineered microorganisms has emerged as a promising and environmentally sustainable alternative to traditional chemical synthesis[11].

Oxalic acid biosynthesis occurs across diverse organisms, including bacteria, fungi, plants, and animals[12]. The filamentous fungus *Aspergillus niger* has long been considered a potent strain for industrial oxalic acid production due to its ability to utilize a wide range of carbon sources, including lactose, sucrose[13], glucose[14], milk whey media[15], whey permeate[16], and crude rapeseed oil[17]. Its extensive use in the citric acid industry further underscores its potential as a microbial chassis for organic acid biosynthesis. However, extending this platform to other acids introduces additional challenges. In submerged fermentation, *A. niger* exhibits highly variable morphologies, ranging from dispersed hyphae to compact pellets, with each form significantly affecting broth rheology, oxygen transfer, and overall productivity[18]. Highly dispersed growth at industrial biomass concentrations generates pseudoplastic, viscous broths that hinder mixing and oxygen delivery, while pellet growth alleviates rheological issues but often produces oxygen-deprived cores susceptible to autolysis. Consistent and scalable pellet formation thus required careful adjustment of inoculum density, medium composition, and hydrodynamics, even in low-shear systems such as rocking-motion bioreactor[19]. Although decades of optimization have mitigated these challenges for citric acid, the different pH optima and metabolic requirements for other organic acids can exacerbate morphology-related limitations.

We developed a microbial platform for oxalic acid biosynthesis. The non-conventional yeast *Issatchenkia orientalis* (also known as *Pichia kudriavzevii*) was selected as the production host owing to its remarkable tolerance to low pH and its inherently unicellular morphology. This capability allows fermentation to proceed under acidic conditions without the need for expensive pH regulation. This low-pH operation is particularly advantageous, as recovery of REEs from ores also requires acidic conditions, making *I. orientalis* a promising chassis for integrated bioprocesses. In conventional systems, poor acid tolerance in many microorganisms necessitates the use of neutralizing agents to maintain a neutral pH, leading to the formation of organic acid salts during fermentation[20]. It has been estimated that over 60% of total production costs in such systems arise from downstream separation and purification[21]. Meanwhile, *I. orientalis* SD108 can grow across a broad pH range (1.5–6.0)[22,23], and it has been explored to produce several organic acids such as succinic acid[22,24], lactic acid[25], and recently malic acid[26]. A diverse range of genetic tools have been developed for *I. orientalis* SD108, including episomal plasmids[27], strong promoters and terminators, CRISPR/Cas9 systems[28], and a landing pad system for multiple copy gene integration[29]. Together, these traits make *I. orientalis* as a robust and cost-effective platform for the sustainable oxalic acid biosynthesis.

In this study, we expand the microbial repertoire for oxalic acid production by establishing *I. orientalis* SD108 as a production chassis. Although this yeast has been engineered to produce several organic acids, its potential for oxalic acid biosynthesis has not been reported. We introduce a synthetic pathway and apply targeted metabolic engineering to enable and enhance oxalic acid formation. Importantly, we couple fermentation output directly with REE precipitation, creating a streamlined process that eliminates the need for downstream purification of oxalic acid. By uniting the acid tolerance and industrial robustness of *I. orientalis* with the geochemical utility of oxalic acid, this work provides a proof-of-concept for using non-conventional yeast to bridge microbial biomanufacturing with critical materials recovery (Fig. 1).

Results

Metabolic engineering of *I. orientalis* for oxalic acid production

There are two reported oxalate biosynthetic pathways in microorganisms, the oxaloacetate cleavage pathway and the glyoxylate oxidation pathway[30–32]. In the former pathway, oxaloacetate hydrolase (Oah) cleaves oxaloacetate into oxalic acid and acetate. For the latter pathway, glyoxylate dehydrogenase (GLOXDH) oxidizes glyoxylate to oxalic acid. Munir et al. demonstrated that Oah is the primary enzyme responsible for producing oxalic acid in the wood-rotting fungus *Fomitopsis palustris*, as its activity is greater than that of GLOXDH[32]. Therefore, we introduced the oxaloacetate cleavage pathway into the low pH tolerant yeast *I. orientalis* SD108. Li et al. previously overexpressed and purified two Oah homologs: Pcoah from *Penicillium chrysogenum*, and Fpoah from *Fomitopsis palustris*. The two enzymes exhibited similar V_{max}/K_m values of 9.41×10^{-4} and 9.05×10^{-4} s^{-1} mg^{-1} protein, respectively[33]. To establish the oxaloacetate cleavage pathway in *I. orientalis* SD108, the codon optimized *Pcoah* and *Fpoah* genes were integrated into the genome of *I. orientalis* SD108 LPB/*Δura3*, a landing pad strain designed to enable simultaneous integration of multiple genes[29]. Both strains were evaluated for oxalic acid production in shake flask fermentation using SC-URA medium with 50 g·L^{-1} glucose. While *I. orientalis* SD108 LPB did not produce oxalic acid, strains expressing *Pcoah* and *Fpoah* produced 0.38 g·L^{-1} and 0.59 g·L^{-1} oxalic acid, respectively (Fig. 2b). To further enhance the titer, we utilized the landing pad system to integrate multiple copies of these genes into the chromosome. The strain expressing three copies of *Pcoah* achieved the highest oxalic acid titer of 1.28 g·L^{-1}, which was named strain OA_Pcoah.

To enhance oxalic acid production, we expressed the endogenous pyruvate carboxylase (PYC) in the strain OA_Pcoah. PYC facilitates the conversion of pyruvate into oxaloacetate (OAA), a precursor of oxalate. We also evaluated whether increasing its copy number would improve the oxalic acid titer. Strains with two and three copies of *PYC* produced a similar oxalic acid titer of 1.52 g·L^{-1} (Supplementary Fig. 1), suggesting that two copies of the *PYC* gene are sufficient for oxalic acid production under these conditions. We then selected the strain with two copies of *PYC* for the next step, resulting in the strain OA_Pcoah_PYC.

To further enhance oxalic acid production, we introduced an oxalate transporter to the engineered strain. Watanabe et al. identified the oxalate transporter gene *FpOAR* from *Fomitopsis palustris*, which facilitates the export of intracellular oxalic acid using ATP in *F. palustris*[34]. Yang et al. later identified two additional oxalate transporters, HbOT1 and HbOT2, from *Hevea brasiliensis*[35]. Each of these

https://doi.org/10.1038/s41467-026-68957-5

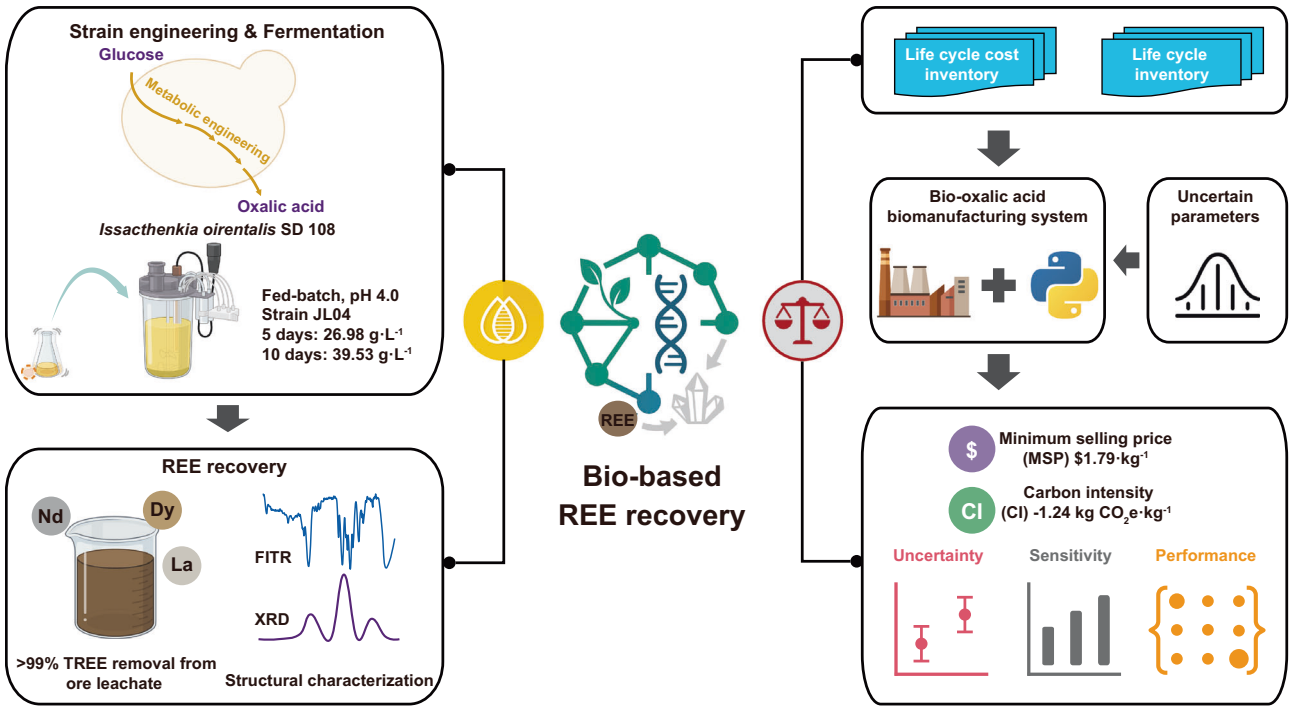

Fig. 1 | Overview of the bio-oxalic acid production and REE recovery using engineered *I. orientalis*. The engineered *I. orientalis* strain produced up to 39.53 g·L^{-1} oxalic acid under low pH fermentation. The crude fermentation broth enabled >99% total rare earth element (TREE) recovery from ore leachate. Techno-economic analysis and life cycle assessment estimated a minimum selling (MSP) of $ 1.79·kg^{-1} and CI of -1.24 kg CO_2e·kg^{-1} at baseline. Figure created using elements from BioRender.com with modification in Adobe Illustrator.

three oxalate transporter genes was codon-optimized and expressed in the strain OA_Pcoah. Among them, the strain expressing *HbOT2* showed higher oxalic acid production compared to the strains harboring *FpOAR* or *HbOT1* (Supplementary Fig. 2). Combining these genetic modifications, the resulting JL01 strain carries three copies of *Pcoah*, two copies of *PYC*, and one copy of *HboT2*. To enhance the oxalic acid titer and evaluate the performance of the engineered strain JL01, we conducted fed-batch fermentation using the bench-top bioreactors. Two pH levels and two dissolved oxygen (DO) conditions were tested. The highest oxalic acid titer, 14.97 g·L^{-1}, was achieved at 10% DO and pH 4.0 (Fig. 2c). Increasing the DO to 20% slightly reduced the titer to 12.48 g·L^{-1}. Similarly, increasing the pH to 6.0 further decreased the titer to 9.66 g·L^{-1} oxalic acid (Supplementary Fig. 3).

During these tests, glycerol was identified as the major byproduct, accumulating to approximately 12.0 g·L^{-1} under the 10% DO and pH 4.0 conditions. Since glycerol-3-phosphate dehydrogenase (GPD) plays a key role in the glycerol biosynthesis pathway, we knocked out the *GPD* gene in strain JL01, generating the strain JL02. Fermentation of strain JL02 yielded a comparable oxalic acid titer of 14.7 g·L^{-1} without any detectable glycerol accumulation (Fig. 2c). Various fermentation conditions, including pH levels (3.0 or 4.0) and DO levels (5%, 10%, or 20%) were tested. Based on the results, the optimal fermentation conditions for oxalic acid production were determined to be pH 4.0 and 10% DO (Supplementary Fig. 4). The fed-batch fermentation of strain JL02 in SC-URA medium with glucose feeding produced 14.72 g·L^{-1} of oxalic acid with a yield of 0.09 g·g^{-1} glucose equivalent and a productivity of 0.12 g·L^{-1}·h^{-1}.

To enhance carbon flux toward the pyruvate branching point, pyruvate kinases were expressed to catalyze the conversion of phosphoenolpyruvate (PEP) to pyruvate. Two candidates were evaluated in strain JL02: PYK1 from *S. cerevisiae* and JL09_g4285 from *I. orientalis*. Under shake flask fermentation, JL02_PYK1 produced 5.95 g·L^{-1} of oxalic acid, while JL02_g4285 achieved a titer of 4.43 g·L^{-1}. The strain JL02_PYK1 was selected for further optimization and renamed JL03. Under fed-batch fermentation, JL03 produced 19.27 g·L^{-1} of oxalic acid with a yield of 0.12 g·g^{-1} glucose equivalent and a productivity of 0.16 g·L^{-1}·h^{-1} (Supplementary Fig. 5).

It has been reported that inositol pyrophosphatase, encoded by *OCA5*, regulates glycolysis and respiration by modulating levels of 5-diphosphoinositol 1,2,3,4,6-pentakisphosphate (5-InsP7). 5-InsP7 acts as an energy sensor, detecting ATP concentrations and balancing gene expression between glycolysis and respiration[36]. We knocked out *g4567*, the homolog of *OCA5*, in strain JL03, generating strain JL04. This modification enhanced oxalic acid production, resulting in a titer of 26.98 g·L^{-1}, with a yield of 0.19 g·g^{-1} glucose equivalent and a productivity of 0.23 g·L^{-1}·h^{-1} (Fig. 2c). We also extended the fermentation time to 10 days, during which strain JL04 produced 39.53 g·L^{-1} oxalic acid with a yield of 0.18 g·g^{-1} glucose equivalent and a productivity of 0.17 g·L^{-1}·h^{-1} (Supplementary Fig. 6).

Bio-oxalic acid for REE recovery: precipitation, structure, and composition

To evaluate the ability of bio-oxalic acid to precipitate REEs, we performed a precipitation assay using the cultured supernatant from strain JL04, which contained 7.80 g·L^{-1} oxalic acid. The supernatant was tested against a neodymium (Nd) chloride solution, alongside commercial oxalic acid from Sigma-Aldrich for comparison. This experiment tests the efficacy of the biologically produced oxalic acid in a scenario of relevance to REE mining, where individually separated REEs are precipitated using oxalic acid on the path to rare earth oxide production. The Nd feed solution was mixed with the oxalic acid solutions at final molar ratios of oxalic acid to Nd ranging from 0 to 6.2. Colorimetric assay revealed that the recovery efficiency of bio-oxalic acid was nearly identical to that of the commercial oxalic acid at all concentrations tested. Specifically, bio-oxalic acid precipitated over 99% of Nd when the molar ratio of oxalic acid to Nd exceeded 2:1 (Fig. 3a). To further demonstrate the applicability of bio-oxalic acid in REE recovery, we repeated the precipitation experiment using the

https://doi.org/10.1038/s41467-026-68957-5

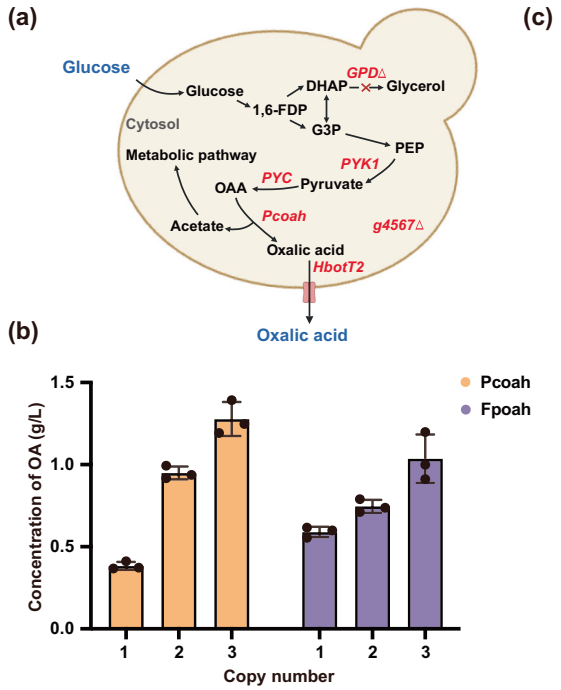

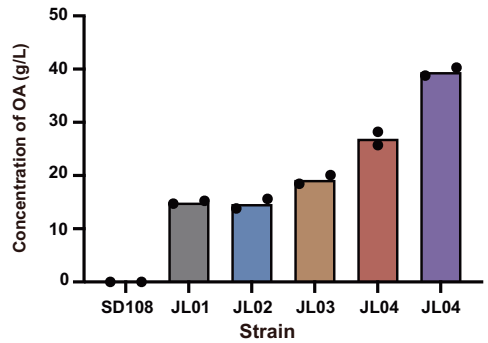

Genetic modification	SD108	JL01	JL02	JL03	JL04	JL04
Pcoah	−	+	+	+	+	+
PYC	−	+	+	+	+	+
HboT2	−	+	+	+	+	+
PYK1	−	−	−	+	+	+
GPD△	−	−	+	+	+	+
g4567△	−	−	−	−	+	+
Fermentation (days)	5	5	5	5	5	10

Fig. 2 | *I. orientalis* as a platform for oxalic acid production. a Schematic of oxalic acid biosynthesis in the engineered *I. orientalis* strain. Deleted genes are indicated by a delta Δ and highlighted in red. Overexpressed genes are also marked in red. Key intermediates and enzymes: 1,6-FDP, fructose-1,6-bisphosphate; G3P, glycerol 3-phosphate; DHAP, dihydroxyacetone phosphate; PEP, phosphoenolpyruvate; OAA, oxaloacetate; GPD, glycerol-3-phosphate dehydrogenase; PYK1, pyruvate kinase; PYC, pyruvate carboxylase; Pcoah, oxaloacetate hydrolase; HboT2, oxalate transporter; g4567, inositol pyrophosphatase. Created with the BioRender.com. **b** Oxalic acid titers in strains expressing *Pcaah* or *Fpoah* with varying copy numbers. Data represent mean ± SD of three independent biological replicates ($n = 3$). **c** Fed-batch fermentation of oxalic acid in engineered strain (JL01 to JL04) and the parental strain (SD108) in a 100 mL bioreactor. Genetic modifications are summarized in the table below. Each point represents an independent biological replicate ($n = 2$). Source data are provided as a Source Data file.

higher concentration supernatant containing 42.70 g·L^{-1} oxalic acid. In addition to $NdCl_3$, we included lanthanum (La) chloride and dysprosium (Dy) chloride, representative light and heavy REEs, respectively, to test the generalizability of the precipitation process. The results show that the bio-oxalic acid could precipitate over >99% of Nd and La, and >98% of Dy at the molar ratios above 2:1 (Supplementary Fig. 7). These findings confirm that the crude, fermentation-derived oxalic acid could effectively recover multiple REEs without the need for purification.

To further test the application relevance of bio-oxalic acid, we conducted precipitation experiments with a pregnant leachate solution derived from a primary REE source (allanite) with the goal of selectively precipitating a high-purity total REE product. Allanite is a REE-bearing silicate mineral found in mineable quantities in many regions, including a large deposit in Wyoming, USA; however, it has not yet been exploited at an industrial scale for REEs[37]. The general formula of allanite is $A_2M_3Si_3O_{12}[OH]$, where site A accommodates REEs, Ca, Sr, Pb, Mn, Th, and U, and site M includes Al, Fe, Mn, Mg, Ti, Cr, and V. The leachate used in this study originated from leaching an allanite concentrate with hydrochloric acid followed by precipitation steps to remove Fe, Al, and Si (see Methods). Hydrogen peroxide was added to oxidize ferrous to ferric followed by a sequence of precipitation steps to remove most of the contaminating Fe, Al, and Si. However, in addition to a high concentration of REEs, the leachate still contained significant amounts of non-REE contaminants such as Ca^{2+}, Al^{3+}, Mn^{2+}, Zn^{2+}, UO_2^{2+}, Th^{4+} (Supplementary Data 1). We evaluated the performance of bio-oxalic acid through precipitation assays using two cultured supernatants containing 22.00 g·L^{-1} and 42.70 g·L^{-1} oxalic acid, respectively and included 1 M commercial oxalic acid as a reference (Fig. 3b and Supplementary Fig. 8). Increasing the oxalic acid dosage improved total REEs (TREE) precipitation efficiency: over 99% TREE precipitation was observed at oxalic acid concentrations above 2.70 g·L^{-1}. Notably, there was no significant difference in precipitation efficiency between the two bio-oxalic acid concentrations tested or between bio-oxalic acid and commercial oxalic acid. Both LREE (defined as Sc, La, Ce, Pr, Nd, and Sm) and HREE (Y, Eu, Gd, Tb, Dy, Ho, Er, Tm, Yb and Lu) were efficiently precipitated with comparable efficiency across all tested conditions. Minimal precipitation of non-REE was observed, with less than 6% precipitation of Ca, Mg, Mn, and Zn (Supplementary Data1). These results demonstrate that bio-oxalic acid enables high REE recovery efficiency, comparable to commercial oxalic acid, even in the presence of non-REE contaminants. Notably, the bio-oxalic acid was used directly from the spent fermentation medium without any downstream purification, and still yielded high-purity REE oxalate precipitates. This highlights a key advantage of the biological process: eliminating the need for downstream processing significantly reduces operational complexity and waste generation but lowers overall production cost.

To further evaluate the suitability of bio-oxalic acid for REE recovery, we analyzed the crystallographic properties of the precipitated REE oxalates using XRD (Fig. 3c, Supplementary Table 3). We compared the structure of $Nd_2(C_2O_4)_3{\cdot}10H_2O$ synthesized using bio-oxalic acid to that produced with commercial oxalic acid, aiming to confirm the quality and structural consistency of the bio-derived product. The XRD patterns show that the $Nd_2(C_2O_4)_3{\cdot}10H_2O$ synthesized using bio-oxalic acid exhibits crystallographic features that closely match those of the commercial oxalic acid. The major diffraction peaks corresponding to the (100), (110), (011), ($\bar{1}11$), ($\bar{1}02$), (111), ($\bar{2}11$), ($\bar{3}02$), and (311) planes, which are characteristic of the $Nd_2(C_2O_4)_3{\cdot}10H_2O$ structure, are present in both samples (Fig. 3c). Notably, the (100) peak at 10.2 Å and the (110) peak at 6.97 Å are the most prominent, representing the primary lattice spacings of the

https://doi.org/10.1038/s41467-026-68957-5

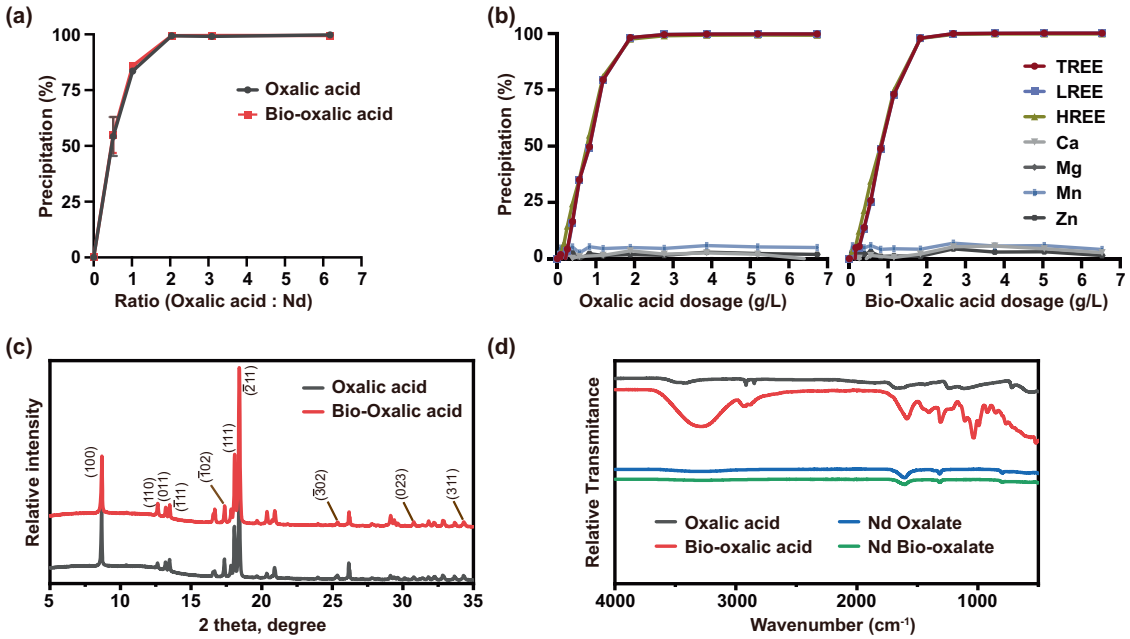

Fig. 3 | Comparable REE recovery efficiency and product characterization between bio-derived and commercial oxalic acid. a Nd-oxalate precipitation using commercial or bio-oxalic acid at varying concentration of 7.80 g·L^{-1}. Data are presented as mean ± SD of three independent precipitation assays ($n = 3$). **b** Effective precipitation of total REEs (TREE) from allanite leachate using bio-oxalic acid (42.70 g·L^{-1} feedstock) and commercial oxalic acid (1 M feedstock, equivalent to 90.03 g·L^{-1}), TREE represent the combination of light REEs (LREE) and heavy REEs (HREE). The LREEs analyzed include Sc, La, Ce, Pr, Nd, and Sm; the HREEs include Y, Eu, Gd, Tb, Dy, Ho, Er, Tm, Yb, and Lu. **c** XRD patterns of $Nd_2(C_2O_4)_3{\cdot}10H_2O$ synthesized using commercial oxalic acid and bio-derived oxalic acid, showing matching diffraction peaks for key planes such as (100), (110), (011), and (111), confirming structural equivalence. **d** FTIR (ATR) spectra of Nd oxalic precipitates produced using bio-derived vs commercial oxalic acid. Source data are provided as a Source Data file.

crystal structure. These peaks exhibit a strong correlation between the bio-oxalic and commercial products, indicating that the overall crystallinity and phase structure of the bio-oxalic sample closely match the commercial-derived material.

While some minor variations in peak intensities are observed, especially in higher-angle regions such as the ($\bar{1}11$), ($\bar{2}11$), and (311) peaks, these differences are not substantial and can be attributed to slight variations in crystallinity, synthesis conditions, or sample purity. For example, the ($\bar{1}11$), and ($\bar{1}02$) peaks, which are also indicative of the compound's crystal structure, show slightly lower intensities in the bio-oxalic sample. However, the d-spacing values for these peaks remain consistent, further supporting the similarity in crystal structure. Overall, the XRD data confirm that the bio-oxalic acid-derived $Nd_2(C_2O_4)_3{\cdot}10H_2O$ retains the same structural integrity and phase composition as the commercial oxalic acid-synthesized material.

Based on the FTIR (ATR) results, both bio-oxalic acid and commercial oxalic acid exhibit similar overall characteristics, indicating a comparable chemical structure (Fig. 3d). However, minor differences suggest the presence of impurity in the bio-oxalic acid. Specifically, bio-oxalic acid shows an additional peak around 1200 cm^{-1}, which could be attributed to C-O stretching vibrations, possibly from residual organic contaminants or by-products of the biosynthesis process. A broad 3400 cm^{-1} peak observed in the bio-oxalic acid is likely associated with O-H stretching vibrations, suggesting the presence of hydroxyl groups from water or alcohols. This indicates that the bio-oxalic acid contains additional moisture or hydroxyl-containing impurities, possibly introduced during the biosynthesis process or sample preparation. These features are absent in the commercial Sigma oxalic acid spectrum, indicating a purer material with lower moisture and organic impurity levels.

When analyzing the Nd oxalic precipitates, both bio- and commercial oxalic acid show similar FTIR spectra, with key peaks at 1600 cm^{-1} and 1350 cm^{-1}, which are characteristic of the C = O stretching vibrations of the oxalate anion ($C_2O_4^{2-}$). A minor peak at 800 cm^{-1} is also observed, likely corresponding to C-O bending vibrations. These peaks confirm that both types of Nd oxalic precipitates contain the same oxalate coordination with Nd^{3+}, indicating that the Nd oxalic precipitate formed using bio-oxalic acid is comparable to that formed with commercial Sigma oxalic acid.

Overall, the results demonstrate that bio-oxalic acid exhibits a comparable efficiency to commercial oxalic acid for REE recovery, as evidenced by precipitation tests using Nd chloride solution and allanite leachates. The XRD and FTIR analyses further confirm the structural and chemical similarities between the two types of oxalic acid, with the bio-derived product achieving high crystallinity and exhibiting only minor impurities. Together, these findings demonstrate the potential of bio-oxalic acid as an effective and sustainable alternative to commercial oxalic acid for REE recovery.

Techno-economic analysis and life cycle assessment

To characterize the financial viability and environmental implications of bio-oxalic acid production, we designed and simulated an end-to-end biomanufacturing facility with sugarcane as a feedstock. Based on an annual production capacity of 127,000 metric tons (the projected 2032 U.S. market size)[38,39], the biomanufacturing facility could produce market-competitive bio-oxalic acid at a minimum selling price (MSP) of \$1.79·kg^{-1} (baseline; Fig. 4a) with a range of \$1.51 to \$2.21·kg^{-1} (5th–95th percentiles, hereafter in brackets). Carbon intensity (CI) was estimated to be −1.24 kg CO_2e·kg^{-1} [-2.83 to 0.02 kg CO_2e·kg^{-1}], representing a reduction of more than 100% relative to fossil-based counterpart (Fig. 4b; a similar trend was observed for fuel energy consumption in Supplementary Fig. 12). This negative CI was due to excess electricity generation from sugarcane bagasse, accounted for using the displacement method (Supplementary Fig. 10). Among the 29 uncertain parameters, MSP was most sensitive to sugarcane price and fermentation yield, with a Spearman's ρ of 0.53 and -0.48, respectively; while CI showed the strongest positive correlation with fermentation yield, with Spearman's ρ of 0.62 (Supplementary Fig. 9).

https://doi.org/10.1038/s41467-026-68957-5

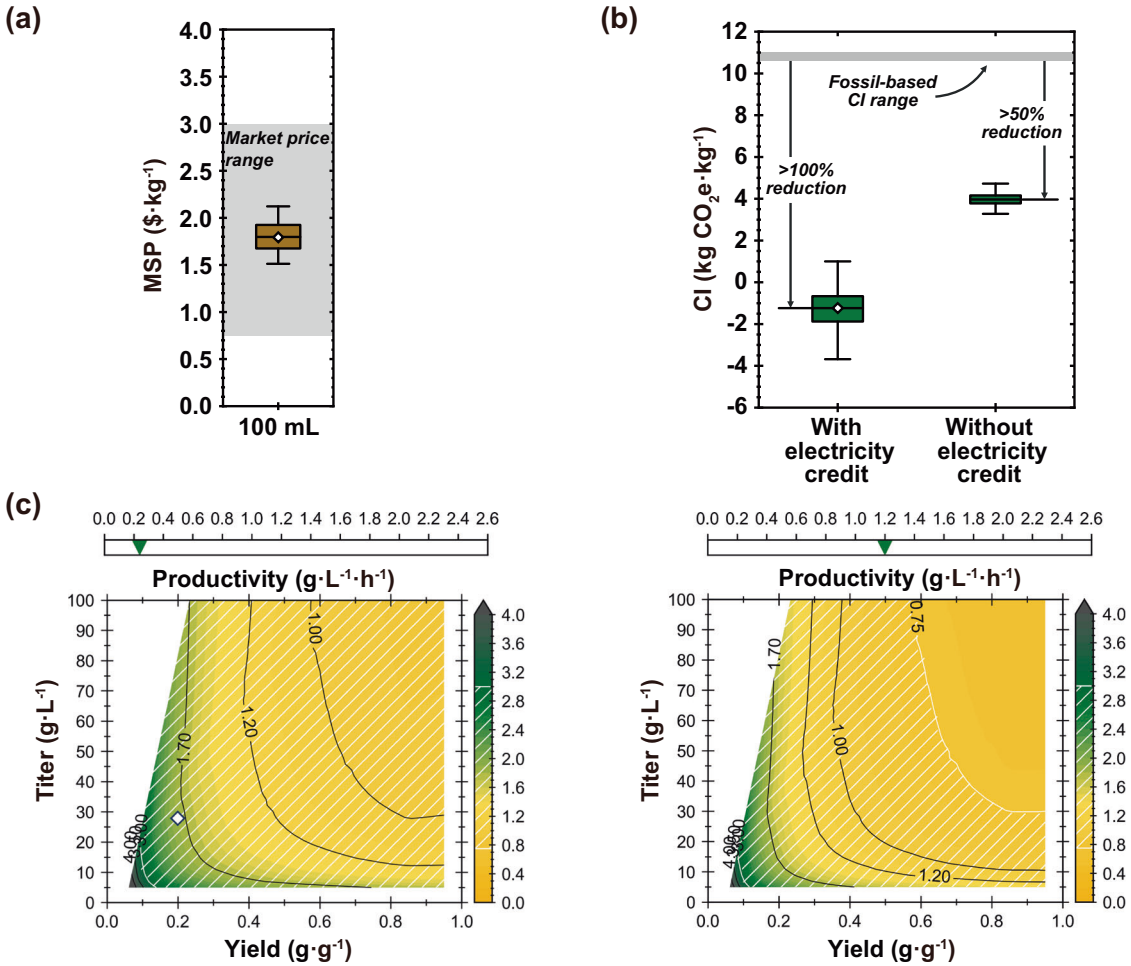

Fig. 4 | Techno-economic analysis and life cycle assessment under uncertainty and across the theoretical fermentation performance space. Uncertainties (box and whisker plots) for **a** minimum selling price (MSP) and **b** cradle-to-grave carbon intensity (CI) with and without electricity credit. Whiskers, boxes, and middle lines represent 5th/95th, 25th/75th, and 50th percentiles from 6,000 Monte Carlo simulations. Diamond markers represent baseline results. Grey shaded areas represent the market price range of oxalic acid ($0.75–3.0 kg^{-1})[38,45] and the CI range of fossil-based oxalic acid (10.6 to 11.0 kg CO_2e·kg^{-1})[46]. **c** MSP across 2,500 fermentation yield-titer combinations at the baseline productivity (0.24 g·L^{-1}·h^{-1}), and a 5-fold improvement. Diamond marker represents the baseline MSP under the baseline yield of 0.2 g·g^{-1} glucose and the baseline titer of 28.23 g·L^{-1} oxalic acid. Source data are provided as a Source Data file.

To further explore the impact of fermentation performance, we conducted TEA and LCA across the theoretical fermentation space and confirmed yield and productivity (i.e., rate) represent key opportunities to drive down MSP (Fig. 4c).

Discussion

Rare earth elements are crucial components in clean energy and advanced electronics technologies. The processes used in respective extraction and separation are environmentally intensive and driven by chemistry. Oxalic acid is commonly used to precipitate REEs during downstream purification, but its production remains heavily reliant on fossil-based feedstocks and energy-intensive synthesis routes[10]. To address these limitations, we aimed to develop a bio-based route for oxalic acid production that eliminates the need for purification, allowing the direct use of fermentation supernatant for REE recovery while maintaining high purity. This streamlined approach improves both process efficiency and economic feasibility.

Among microbial hosts explored for oxalic acid production, *A. niger* has been the most widely studied due to its high titers and ability to utilize diverse carbon sources. Reported concentrations range from ~15 to 123 g·L^{-1} across substrate and fermentation strategies, with the highest titer (122.7 g·L^{-1}) achieved under optimized submerged shake-flask fermentation using cashew apple juice at pH 5.4[13–17,40–44]. However, the large-scale application of *A. niger* represents several problems: it is sensitive to pH fluctuations, exhibits high oxygen demand, and its filamentous growth complicates broth rheology quite complex. Moreover, *A. niger* W78 C typically co-produces large amount of citric acid and gluconic acid alongside oxalic acid, particularly under sub-optimal conditions. Both are strong rare-earth-chelating agents and are expected to compromise REE precipitation efficiency when present. Even at pH 6.0, where oxalate production is highest, the selective chemical yield achieved was only 58.6%, thereby reducing overall process efficiency of the global process and complicating downstream separation[41]. Representative examples of oxalic acid production by various microorganisms reported in the literature are summarized in Supplementary Table 4.

In this study, we engineered the non-model yeast *I. orientalis* to produce oxalic acid for REE recovery. To establish oxalic acid biosynthesis in *I. orientalis*, we screened two Oah candidates and integrated them with different gene copy numbers in a single step. To facilitate oxalic acid export, we tested three oxalic acid transporters. Additionally, knocking out *GPD1* and *OCA5* homologs reduced byproduct accumulation and improved oxalic acid titer. Further enhancement was achieved by overexpressing *PYC* and *PYK1*,

effectively redirecting metabolic flux toward OAA. These combined modifications result in a final strain capable of producing 39.53 g·L^{-1} of oxalic acid with a yield of 0.18 g·g^{-1} glucose equivalent under fed-batch fermentation conditions. To date, we have developed *I. orientalis* as a chassis microbial system to produce oxalic acid that integrates acid tolerance with genetic accessibility and the capability for scaled fermentation. Indeed, *I. orientalis* has already demonstrated production levels of succinic acid as high as 63.1 g·L^{-1} in pilot-scale batch fermentation, suggesting the potential for industrial bioproduction[24].

Therefore, after fermentation, the cell pellet could be discarded by simply centrifugation, and the supernatant containing the bio-oxalic acid could be used directly for REE precipitation without any downstream purification. The bio-oxalic acid achieved >99% precipitation of Nd^{3+} and La^{3+}, and >98% for Dy^{3+} at oxalate-to-REE molar ratios above 2:1, comparable to commercial oxalic acid. When tested with an allanite leachate containing both REEs and non-REE contamination such as Ca^{2+}, Fe^{3+}, Al^{3+}, and Na^{+}. The process maintained over 99% total REE recovery at concentration above 2.70 g·L^{-1}, demonstrating robustness even in complex matrices. It is worth noting that metals present in the fermentation broth are typically at lower concentrations and dominated by monoanions, in contrast to the multivalent metal species in ore leachates (Ca^{2+}, Fe^{3+}, Al^{3+}). As a result, their impact on REE precipitation is minimal, as reflected by the comparable purity of REE oxalates produced using bio-derived and commercial oxalic acids.

In the proposed process, oxalic acid is synthesized by *I. orientalis* in a bioreactor under optimal conditions. After fermentation, the biomass is separated by centrifugation and the supernatant rich in oxalic acid is directly utilized as a REE precipitation agent, enabling efficient and high-purity REE precipitation in two scenarios relevant to REE mining: precipitation from an individual REE chloride solution in downstream REE purification and from an acid leachate solution in an upstream process step before individual REE separation. This two-stage approach overcomes the major challenges of in situ precipitation, including REE-induced inhibition of cell growth and oxalic acid production, as well as the difficulty of recovering REEs from the cell biomass. Importantly, the separation step also opens the possibility for developing a continuous or semi-continuous bioprocess, which could help alleviate product inhibition, enhance process stability, and improve overall productivity. Future work should address scalability, process integration with upstream leaching operations, long-term reactor performance under industrial conditions, and expansion of this approach to a broader range of REE sources.

We conducted TEA and LCA to evaluate the economic feasibility and life cycle environmental impacts of bio-oxalic acid production against the fossil-based benchmark. The biomanufacturing facility achieved a market competitive MSP of \$1.79·kg^{-1} [\$1.51 to 2.12·kg^{-1}], well within the reported market price range of \$0.75 to 3.0·kg^{-1} [38,45]. Further, carbon-negative bio-oxalic acid production is possible in support of REE recovery, with CIs of -1.24 kg CO_2e·kg^{-1} [-2.83 to 0.02 kg CO_2e·kg^{-1}] as compared to fossil-based oxalic acid (10.6 to 11.0 kg CO_2e·kg^{-1})[46]. The negative CI was achieved through a > 50% reduction in life cycle GHG emissions, along with excess electricity generation from the bio-based feedstock. Increasing fermentation yield and productivity remain the most effective ways to further reduce MSP; a yield increase to 0.24 g·g^{-1} (from the baseline of 0.2 g·g^{-1}) would result in a 7.8% reduction in MSP to \$1.65·kg^{-1}, and a 5-fold increase in productivity to 1.2 g·L^{-1}·h^{-1} would drop MSP by 14% to \$1.54·kg^{-1} at baseline yield and titer (a 10-fold increase in productivity yielded similar results to a 5-fold increase; Supplementary Fig. 13). Given the bio-oxalic acid supernatant can be directly used for REE recovery, there are limited sustainability benefits to increasing maximum titer. Looking ahead, combining higher fermentation performance with favorable feedstock economics (e.g., those of *A. niger*[44]) can further improve the financial viability of bio-oxalic acid production and accelerate its potential role in sustainable REE recovery (Supplementary Fig. 14).

The metabolic flux could be further improved by adaptive evolution, fermentation optimization, or engineering the regulatory network to increase oxalic acid titer and yield. Alternative and inexpensive feedstocks such as sugarcane juice, xylose-rich hydrolysates, or industrial byproducts like corn steep liquor (CSL) could further reduce production costs and support sustainable operation at scale. While this study demonstrated its feasibility at the laboratory level, scaling up will also require addressing key challenges such as strain robustness under industrial conditions (e.g., tolerance to oxalic acid accumulation and growth in complex media) and effective integration of continuous REE precipitation. Overcoming these challenges will be critical to realizing fully integration into a cost-effective, resource-efficient biorefinery for REE recovery.

In conclusion, the key innovation of this work lies in the development and demonstration of an end-to-end pipeline for REE recovery. We engineered a low-pH-tolerant *I. orientalis* strain to biosynthesize oxalic acid, and directly applied the resulting fermentation supernatant for cost-effective REE recovery without purification. Additionally, TEA and LCA underscored the financial viability and environmental benefits of this bioprocess, reinforcing its potential as a sustainable alternative to chemically synthesized oxalic acid. By leveraging yeast as a genetically tractable and scalable microbial host, this study establishes a foundation for cost-effective, industrial-scale oxalic acid production, with applications in REE recovery and a broader portfolio of industrial processes.

Method

Strains, media, and chemicals

All strains used in this study were listed in Supplementary Table 1. *E. coli* DH5α was used to maintain and amplify plasmids and was grown in Luria Bertani medium (1% tryptone, 0.5% yeast extract, 1% NaCl) at 37 °C with ampicillin (100 ug·mL^{-1}). *S. cerevisiae* YSG50 and *I. orientalis* SD108 were propagated in Yeast-Peptone-Dextrose (YPD) medium consisting of 1% yeast extract, 2% peptone, and 2% glucose. Recombinant *I. orientalis* strains were grown in Synthetic Complete (SC) dropout medium lacking uracil (SC-URA). LB broth, bacteriological grade agar, yeast extract, peptone, yeast nitrogen base (w/o amino acid and ammonium sulfate), and ammonium sulfate were obtained from Difco (BD, Sparks, MD), while synthetic complete supplement mixture of amino acids without uracil was obtained from MP Biomedicals (Solon, OH). All restriction endonucleases, Q5 DNA polymerase, and Phusion polymerase were purchased from New England Biolabs (Ipswich, MA). The QIAprep spin mini-prep kit and RNA isolation mini kit were purchased from Qiagen (Valencia, CA), whereas Zymoclean Gel DNA Recovery Kit and Zymoprep Yeast Plasmid Miniprep Kits were purchased from Zymo Research (Irvine, CA). Oxalic acid dihydrate (≥99.5%), neodymium (III) chloride hexahydrate (99.9%), dysprosium (III) chloride hexahydrate (99.9%), and lanthanum (III) chloride heptahydrate (99.9%) were purchased from Sigma-Aldrich (St. Louis, MO). All other chemicals and consumables were purchased from Sigma-Aldrich (St. Louis, MO), VWR (Radnor, PA), and Fisher Scientific (Pittsburgh, PA). Oligonucleotides including gBlocks and primers were all synthesized by Integrated DNA Technologies and Twist Biosciences (IDT, Coralville, IA; Twist Biosciences, San Francisco, CA).

Plasmids and strains construction

The plasmids are listed in Supplementary Table 2, and the primers are provided in the Supplementary Data 5. Genes were codon optimized and synthesized by Twist Bioscience (San Francisco, CA). The amino sequences of proteins used in this study are provided in the Supplementary Data 5. For plasmid construction, Gibson assembly was used[47]. For strain construction, the CRISPR method was adopted to do the gene integration/deletion, and the lithium acetate-mediated method

was used for transformation[48]. Detailed plasmid and strain construction are described in Supplementary Method 1 and Supplementary Method 2.

Shake-flask fermentation and DASbox fed-batch fermentation

For shake flask fermentations, single colonies of *I. orientalis* strains were inoculated into 2 mL of liquid YPD medium with 20 g·L^{-1} of glucose and cultured at 30 °C for 1 day. Then, the cells were subcultured into 50 mL SC-URA medium with 50 g·L^{-1} of glucose in 250 mL Erlenmeyer flask. The initial OD_{600} was 0.2, and the cell were cultivated at 30 °C for 5 days. The samples were collected at day 5 for HPLC analysis. Shake flask fermentations were conducted with three biological replicates.

For fed-batch fermentations in bench-top bioreactors (DASbox, Eppendorf, Hamburg, Germany), single colonies of *I. orientalis* strains were inoculated into 2 mL liquid YPD medium with 20 g·L^{-1} of glucose and cultured for 1 day. 1 mL of cells was then added into 100 mL of liquid SC-URA medium containing 50 g·L^{-1} glucose in the bioreactor. The cells were cultivated at 30 °C and the DO was set to 10%. A cascade program was used to maintain DO by changing RPM, O_2 concentration and then O_2 flow rate. pH was maintained at 4.0 using 4 N HCl and 4 N KOH. One drop of Antifoam 204 (Sigma-Aldrich, USA) was added to control foaming if necessary. After the initial glucose was depleted, additional glucose was added to the bioreactors. Samples were collected every 24 hours for HPLC analysis. Fed-batch fermentations were conducted with two biological replicates.

Precipitation test

Bio-oxalic acid samples were collected from the different stages of JL04 fermentation. Culture was centrifuged at 8,000 × g for 30 min to separate the supernatant from cell pellet. We tested a bio-oxalic acid containing 7.8 g·L^{-1} oxalic acid for REE precipitation. For comparison, commercial oxalic acid was used as a reference. To match the bio-oxalic acid concentrations, 1.09 g of oxalic acid dihydrate were dissolved in 10 mL of deionized (DI) water, yielding solutions of 7.8 g·L^{-1}. Neodymium (III) chloride hexahydrate was dissolved in 1 mM HCl to prepare a 50 mM Nd stock solution. The stock solution was subsequently diluted with 10 mM HCl to achieve a final concentration of 1 mM, which was used as the REE feed solution for the precipitation tests. The Nd feed solution and oxalic acid solutions were mixed to achieve final oxalic acid-to-neodymium (oxalic acid:Nd) molar ratios ranging from 0 to 6.2. The mixtures were allowed to sit overnight to facilitate precipitation. Following this, the samples were centrifuged at 1,000 × g for 5 min to separate the precipitate from the supernatant. The supernatants were collected, and the neodymium concentrations were analyzed using a xylenol orange colorimetric assay[49]. Briefly, 40 µL of pre-diluted sample (1–200 µM) was mixed with 120 µL of 0.5 M MES buffer (pH 6), followed by the addition of 40 µL of 1 mM xylenol orange in 0.5 M MES buffer (pH 6). Absorbance was measured at 580 nm, and Nd concentrations were determined by comparison to standard curves.

A higher concentration of bio-oxalic acid (42.70 g·L^{-1}) was subsequently used to evaluate its applicability in REE recovery. In addition to Nd, stock solutions of dysprosium (III) chloride hexahydrate and lanthanum (III) chloride heptahydrate were prepared by dissolving each salt in 1 mM HCl to a final concentration of 50 mM. These stock solutions were further diluted in 10 mM HCl to a working concentration of 1 mM, which served as the REE feed solution for precipitation assays. Bio-oxalic acid or commercial oxalic acid was added to the REE feed solutions to achieve final oxalic acid-to-REE molar ratios ranging from 0 to 3. The mixtures were incubated overnight at room temperature to allow complete precipitation. Samples were then centrifuged at 1000 × g for 5 min to separate the precipitate from the supernatant. REE concentrations were analyzed using a xylenol orange colorimetric assay.

To perform oxalic acid tests on leach liquor produced from a primary source, allanite ore was obtained from the Halleck Creek, Wyoming deposit containing 0.32% total REEs. The ore sample was ground to a top particle size of 1 mm and concentrated to 1.67% total REEs in the sink fraction of a lithium metatungstate (LMT) dense medium having a specific gravity (SG) of 2.95. The material heavier than 2.95 SG was further ground to a top size of 150 microns. The ground ore was leached in a hydrochloric acid solution heated to 75 °C and containing 30% solids by weight at an acid-to-solid ratio of 0.3:1.0 for two hours. To oxidize the ferrous iron to ferric iron, hydrogen peroxide was added to the leach liquor at a dosage equal to 0.6% by volume; the progress was monitored via redox potential measurements to ensure complete oxidation. The pH of the leach liquor was raised to a value of 2.5 by the addition of 5 M NaOH to precipitate and remove iron and silica gel by filtration. Afterwards, the solution pH was further increased to pH 4.5 to precipitate and remove aluminum followed by the precipitation of the REEs at pH 8.0. The REE precipitate cake was redissolved by the incremental addition of 12 M HCl and diluted to make 310 mL of oxalate precipitation feed aqueous. The solution was filtered to remove manganese hydroxide. A 1 M solution of commercial oxalic acid and a bio-oxalate solution were then added to the solution in separate test programs while mixing and adding 5 M sodium hydroxide to maintain the solution pH at 1.5. The precipitated RE oxalate was recovered by centrifugation and filtration. For the elemental analysis of solids, samples were digested using a combination of aqua regia and hydrofluoric acid following the procedure described in ASTM D6357. A sample of 100 mg were digested in 20 mL of aqua regia and 20 mL of hydrofluoric acid at 150 °C till all liquids evaporated. Next, 11 mL of nitric acid and 20 mL of deionized water were added to the digestion tube and digested at 120 °C until a total volume of 10 mL remained. The liquid volume was diluted with 20 mL of deionized water in preparation for inductively coupled plasma optical emission spectroscopy (ICP-OES) analysis. For the digested liquid and leachates, a single independent sample was prepared and analyzed for each condition ($n = 1$).

REE recovery efficiency was calculated based on the decrease in REE concentration in the supernatant following oxalate-induced precipitation. Specifically, recovery was defined as:

$$\text{REE Recovery}(\%) = \left(\frac{C_{\text{feed}} - C_{\text{supernatant}}}{C_{\text{feed}}}\right) \times 100 \quad (1)$$

Where C_{feed} is the initial concentration of REE ions in the feedstock solution prior to oxalic acid addition, and $C_{\text{supernatant}}$ is the concentration of REE ions remaining in the supernatant after precipitation and centrifugation. This approach was applied consistently across all precipitation experiments, including those using commercial or bio-derived oxalic acid at varying concentrations. REE concentrations in the supernatant were quantified using ICP-OES or xylenol orange colorimetric assay, as described above. Since the measurements were based solely on the residual REE in the liquid phase, this method avoids potential overestimation of recovery due to co-precipitation of non-REE metal impurities present in the fermentation broth.

Analytic methods

For quantification of glucose consumption, Agilent 1200 HPLC system equipped with a refractive index detector (Agilent Technologies, Wilmington, DE, USA) and Rezex ROA-Organic Acid H+ (8%) column (Phenomenex, Torrance, CA, USA) were used. The column and detector were run at 50 °C, and 0.005 N H_2SO_4 was used as the mobile phase at a flow rate of 0.6 mL/min[24]. For quantification of oxalic acid production, Shimadzu HPLC with a UV-Vis detector and Aminex HPX-87H Column #1250140 (BioRad, USA) were used. The column was run at 60 °C with 0.005 N H_2SO_4 at a flow rate of 0.6 mL/min and 210 nm was used as the detecting wavelength. This method was adapted from

the work established by Musiał et al., with a slight modification of the column temperature to 60 °C[42].

The REE contents of the digested liquid and leachates were analyzed using ICP-OES system (ARCOS II, Spectro Ametek; model FHX3X, serial number 17006893). The ICP-OES unit was calibrated using four liquid standards having the following concentrations of 0 ppm, 0.2 ppm, 1.0 ppm and 10.0 ppm. The calibration was verified by two independently sourced check standards at the frequency of not less than every 20 samples. The recovery of the check standards was maintained within ±10% RSD. The standard deviation for the total REE content analyses of all samples was less than 5 ppm on a whole sample basis.

All X-ray diffraction (XRD) measurements were performed on a Bruker D8 Advance diffractometer equipped with a Cu Kα radiation. Samples were air-dried prior to analysis. XRD patterns were collected with a step size of 0.015° and a counting time of 3 s per step over a 2θ range up to approximately 65°. The instrument alignment was verified prior to measurements using a corundum standard. Fourier transform infrared (FTIR) spectra were recorded with a Nicolet Summit FTIR spectrometer (ThermoFisher, USA) using a diamond-ATR sample module. Each acquisition was the average of 64 scans (650–4000 cm^{-1}) and was background corrected.

Techno-economic analysis (TEA) and life cycle assessment (LCA)

To assess the economic feasibility and environmental performance of producing bio-oxalic acid from sugarcane (Supplementary Fig. 11), we performed system design, TEA, and LCA under uncertainty in BioSTEAM, an open-source Python-based platform[50,51]. The bio-oxalic acid production facility was assumed to be co-located with REE facilities[52,53]; subsequently, transport burdens were not included in the main analysis. Bio-oxalic acid transport distances of 80 km would increase MSP by ~16.7% and CI by ~2.9% (without electricity credit), with distances up to 324 km still resulting in MSPs within the market price range and well below fossil-based CIs (Supplementary Fig. 15a and 15b). The primary TEA metric was minimum selling price (MSP; in $2016 with a 10% internal rate of return) of bio-oxalic acid on a per-kilogram (kg) basis, calculated from material and energy balances generated by process design and simulations (the unit design and process flowsheet are reported in Supplementary Data 2 and 3, respectively; assumptions for TEA and baseline inventory prices are provided in Supplementary Table 5 and 6, respectively). LCA followed an attributional approach consistent with ISO 14040/44 standard[54,55]. The functional unit was 1 kg of bio-oxalic acid, with impact indicators including cradle-to-grave carbon intensity (CI)[56,57] and fossil energy consumption (FEC). Consistent with Canada's Clean Fuel Regulations[58] and EU's Renewable Energy Directive II[59], indirect land use change impacts were excluded, as they are highly model-dependent, uncertain, and not directly attributable to process-level operations[60]. CI was quantified using the IPCC 2013 Global Warming Potential method (100-year time horizon, GWP_{100})[61] and FEC was assessed using the cumulative energy demand method. To address multifunctionality, the system expansion (or displacement) method was applied for co-product electricity and gypsum. Life cycle inventory data were sourced from ecoinvent v3.8[62] and GREET 2023[63]. To ensure statistical robustness while maintaining computational efficiency, uncertainty analysis was executed via 6,000 Monte Carlo simulations with Latin hypercube sampling (the resulting distributions at alternative samples are reported in Supplementary Table 7 and Supplementary Data 6, demonstrating reproducible results with 6,000 simulations; distributions of all uncertain parameters are listed in Supplementary Data 4). Spearman's rank order correlation coefficients ρ were used to identify key drivers of uncertainty. The Python scripts for BioSTEAM and the biomanufacturing design and analyses are available online[64].

Data analysis

Data analysis was performed using Microsoft Excel and GraphPad Prism 9. Shake flask experiments were conducted with three independent biological replicates ($n = 3$), while bioreactor experiments included two independent replicates ($n = 2$). Figures were generated using GraphPad Prism 9 and finalized in Adobe Illustrator.

Statistics and reproducibility

No statistical method was used to predetermine sample size. Sample sizes were chosen based on experimental feasibility and consistency with standard practice in microbial fermentation and precipitation assays. No data were excluded from the analyses. Experiments were not randomized. Investigators were not blinded to allocation during experiments or outcome assessment. Experiments were repeated as described in the figure legends, with the number of independent replicates indicated for each experiment.

Reporting summary

Further information on research design is available in the Nature Portfolio Reporting Summary linked to this article.

Data availability

All data supporting the findings of this study are available within the paper, its Supplementary Information files, and the Source Data file. Source data are provided with this paper.

Code availability

Python scripts for BioSTEAM and the biomanufacturing facility design as well as analyses can be found on Github at https://github.com/BioSTEAMDevelopmentGroup/Bioindustrial-Park/tree/master/biorefineries/oxalic[64].

References

1. Tyler, G. Rare earth elements in soil and plant systems-A review. *Plant Soil* **267**, 191–206 (2004).
2. Gielen, D. & Lyons, M. Critical materials for the energy transition: Rare earth elements. *International Renewable Energy Agency, Abu Dhabi*, 1-48 (2022).
3. Zhanheng, C. Global rare earth resources and scenarios of future rare earth industry. *J. Rare Earths* **29**, 1–6 (2011).
4. Han, K. N. Characteristics of precipitation of rare earth elements with various precipitants. *Minerals* **10**, 178 (2020).
5. Chi, R. & Xu, Z. A solution chemistry approach to the study of rare earth element precipitation by oxalic acid. *Metall. Mater. Trans. B* **30**, 189–195 (1999).
6. Nawab, A., Yang, X. & Honaker, R. Parametric study and speciation analysis of rare earth precipitation using oxalic acid in a chloride solution system. *Miner. Eng.* **176**, 107352 (2022).
7. Silva, R. G., Morais, C. A., Teixeira, L. V. & Oliveira, ÉD. Selective precipitation of high-quality rare earth oxalates or carbonates from a purified sulfuric liquor containing soluble impurities. *Min. Metall. Explor.* **36**, 967–977 (2019).
8. Amenaghawon, A. N. et al. A comprehensive review of recent advances in the applications and biosynthesis of oxalic acid from bio-derived substrates. *Environ. Res.*, 118703 (2024).
9. Precedence Research. Oxalic Acid Market Size, Share, and Trends 2024 to 2034. https://www.precedenceresearch.com/oxalic-acid-market (2024).
10. Schuler, E., Demetriou, M., Shiju, N. R. & Gruter, G. J. M. Towards sustainable oxalic acid from CO2 and biomass. *ChemSusChem* **14**, 3636–3664 (2021).
11. Liu, H. et al. Recent advances and perspectives on production of value-added organic acids through metabolic engineering. *Biotechnol. Adv.* **62**, 108076 (2023).

12. Grąz, M. Role of oxalic acid in fungal and bacterial metabolism and its biotechnological potential. *World J. Microbiol. Biotechnol.* **40**, 178 (2024).
13. Strasser, H., Burgstaller, W. & Schinner, F. High-yield production of oxalic acid for metal leaching processes by Aspergillus niger. *FEMS Microbiol. Lett.* **119**, 365–370 (1994).
14. Mandal, S. K. & Banerjee, P. C. Submerged production of oxalic acid from glucose by immobilized Aspergillus niger. *Process Biochem* **40**, 1605–1610 (2005).
15. Bohlmann, J., Cameselle, C., Nunez, M. & Lema, J. Oxalic acid production by Aspergillus niger: Part II: Optimisation of fermentation with milk whey as carbon source. *Bioprocess Eng* **19**, 337–342 (1998).
16. Brown, K., Harrison, J. & Bowers, K. Production of oxalic acid from Aspergillus niger and whey permeate. *Water Air Soil Pollut* **229**, 1–10 (2018).
17. Rymowicz, W. & Lenart, D. Oxalic acid production from lipids by a mutant of Aspergillus niger at different pH. *Biotechnol. Lett.* **25**, 955–958 (2003).
18. Paul, G., Priede, M. & Thomas, C. Relationship between morphology and citric acid production in submerged Aspergillus niger fermentations. *Biochem. Eng. J.* **3**, 121–129 (1999).
19. Kheirkhah, T., Neubauer, P. & Junne, S. Controlling Aspergillus niger morphology in a low shear-force environment in a rocking-motion bioreactor. *Biochem. Eng. J.* **195**, 108905 (2023).
20. Tan, S.-I., Liu, Z., Tran, V. G., Martin, T. A. & Zhao, H. Issatchenkia orientalis as a platform organism for cost-effective production of organic acids. *Metab. Eng*. (2025).
21. Li, Q.-Z. et al. Recovery processes of organic acids from fermentation broths in the biomass-based industry. *J. Microbiol. Biotechnol*. (2016).
22. Xiao, H., Shao, Z., Jiang, Y., Dole, S. & Zhao, H. Exploiting Issatchenkia orientalis SD108 for succinic acid production. *Microb. cell fact.* **13**, 1–11 (2014).
23. Wu, Z.-Y. et al. Metabolic engineering of low-pH-tolerant non-model yeast, Issatchenkia orientalis, for production of citramalate. *Metab. Eng. Commun.* **16**, e00220 (2023).
24. Tran, V. G. et al. An end-to-end pipeline for succinic acid production at an industrially relevant scale using Issatchenkia orientalis. *Nat. Commun.* **14**, 6152 (2023).
25. Park, H. J. et al. Low-pH production of d-lactic acid using newly isolated acid tolerant yeast Pichia kudriavzevii NG7. *Biotechnol. Bioeng.* **115**, 2232–2242 (2018).
26. Xi, Y. et al. Metabolic engineering of the acid-tolerant yeast Pichia kudriavzevii for efficient L-malic acid production at low pH. *Metab. Eng.* **75**, 170–180 (2023).
27. Cao, M. et al. A genetic toolbox for metabolic engineering of Issatchenkia orientalis. *Metab. Eng.* **59**, 87–97 (2020).
28. Tran, V. G., Cao, M., Fatma, Z., Song, X. & Zhao, H. Development of a CRISPR/Cas9-based tool for gene deletion in Issatchenkia orientalis. *Msphere* **4**, 00345–00319 (2019).
29. Fatma, Z., Tan, S.-I., Boob, A. G. & Zhao, H. A landing pad system for multicopy gene integration in Issatchenkia orientalis. *Metab. Eng.* **78**, 200–208 (2023).
30. Kobayashi, K., Hattori, T., Honda, Y. & Kirimura, K. Oxalic acid production by citric acid-producing Aspergillus niger overexpressing the oxaloacetate hydrolase gene oahA. *J. Ind. Microbiol. Biotechnol.* **41**, 749–756 (2014).
31. Akamatsu, Y. & Shimada, M. Partial purification and characterization of glyoxylate oxidase from the brown-rot basidiomycete Tyromyces palustris. *Phytochemistry* **37**, 649–653 (1994).
32. Munir, E., Yoon, J. J., Tokimatsu, T., Hattori, T. & Shimada, M. A physiological role for oxalic acid biosynthesis in the wood-rotting basidiomycete Fomitopsis palustris. *Proc. Natl. Acad. Sci. USA.* **98**, 11126–11130 (2001).
33. Li, W. et al. Biosynthesis of plant hemostatic dencichine in Escherichia coli. *Nat. Commun*. **13**, https://doi.org/10.1038/s41467-022-33255-3 (2022).
34. Watanabe, T. et al. Oxalate efflux transporter from the brown rot fungus Fomitopsis palustris. *Applied and environmental microbiology* **76**, 7683–7690 (2010).
35. Yang, Z. et al. Cloning, Expression Analysis, and Functional Characterization of Candidate Oxalate Transporter Genes of HbOT1 and HbOT2 from Rubber Tree (Hevea brasiliensis). *Cells* **11**, 3793 (2022).
36. Qin, N. et al. Flux regulation through glycolysis and respiration is balanced by inositol pyrophosphates in yeast. *Cell* **186**, 748–763 e715 (2023).
37. Xiao, Z. & Zhang, W. Review of allanite: Properties, occurrence and mineral processing technologies. *Green Smart Min. Eng*. (2024).
38. Research Nester. Oxalic Acid Market Size & Share, by Application (Bleaching/Cleaning, Pharmaceuticals, Water Treatment, Textile Dyeing, Metal Leaching, Others) - Global Supply & Demand Analysis, Growth Forecasts, Statistics Report 2025-2037. https://www.researchnester.com/reports/oxalic-acid-market/7493 (2025).
39. U.S. Department of Agriculture, Agricultural Marketing Service. *Oxalic acid dihydrate* https://www.ams.usda.gov/rules-regulations/organic/petitioned-substances/oxalic-acid-dihydrate (2025).
40. Cameselle, C., Bohlmann, J., Nunez, M. & Lema, J. Oxalic acid production by Aspergillus niger: Part I: Influence of sucrose and milk whey as carbon source. *Bioprocess Eng* **19**, 247–252 (1998).
41. Walaszczyk, E., Podgórski, W., Janczar-Smuga, M. & Dymarska, E. Effect of medium pH on chemical selectivity of oxalic acid biosynthesis by Aspergillus niger W78C in submerged batch cultures with sucrose as a carbon source. *Chem. Pap.* **72**, 1089–1093 (2018).
42. Musiał, I., Cibis, E. & Rymowicz, W. Designing a process of kaolin bleaching in an oxalic acid enriched medium by Aspergillus niger cultivated on biodiesel-derived waste composed of glycerol and fatty acids. *Appl. Clay Sci.* **52**, 277–284 (2011).
43. André, A. et al. Biotechnological conversions of bio-diesel derived waste glycerol into added-value compounds by higher fungi: production of biomass, single cell oil and oxalic acid. *Ind. Crops Prod.* **31**, 407–416 (2010).
44. Betiku, E., Emeko, H. A. & Solomon, B. O. Fermentation parameter optimization of microbial oxalic acid production from cashew apple juice. *Heliyon* **2** (2016).
45. Alibaba.com. High-quality oxalic acid CAS 144-62-7. https://www.alibaba.com/product-detail/High-quality-Oxalic-acid-CAS-144_1600467879003.html?spm=a2700.7724857.0.0.737f3dddErELOM (2025).
46. https://ecoinvent.org/ (2025). ecoinvent. ecoinvent.
47. Gibson, D. G. et al. Enzymatic assembly of DNA molecules up to several hundred kilobases. *Nat. Methods* **6**, 343–345 (2009).
48. Gietz, R. D., Schiestl, R. H., Willems, A. R. & Woods, R. A. Studies on the transformation of intact yeast cells by the LiAc/SS-DNA/PEG procedure. *Yeast* **11**, 355–360 (1995).
49. Havel, J., Moreno, C., Hrdlička, A. & Valiente, M. Spectrophotometric determination of rare earth elements by flow injection analysis based on their reaction with xylenol orange and cetylpyridinium bromide. *Talanta* **41**, 1251–1254 (1994).
50. Cortes-Pena, Y., Kumar, D., Singh, V. & Guest, J. S. BioSTEAM: a fast and flexible platform for the design, simulation, and techno-economic analysis of biorefineries under uncertainty. *ACS Sustain. Chem. Eng.* **8**, 3302–3310 (2020).
51. Cortés-Peña, Y. Thermosteam: BioSTEAM's premier thermodynamic engine. *J. Open Source Softw.* **5**, 2814 (2020).
52. Lynas Rare Earths. U.S. project update. https://lynasrareearths.com/u-s-project-update/ (2025).
53. MP Materials. Mountain Pass. https://mpmaterials.com/mountain-pass (2025).

54. ISO. ISO 14040:2006(en) Environmental management — Life cycle assessment — Principles and framework. https://www.iso.org/obp/ui/#iso:std:iso:14040:ed-2:v1:en (2006).
55. ISO. ISO 14044: Environmental Management, Life Cycle Assessment, Requirements, and Guidelines. https://www.iso.org/standard/38498.html (2006).
56. California Air Resources Board. LCFS Pathway Certified Carbon Intensities. https://ww2.arb.ca.gov/resources/documents/lcfs-pathway-certified-carbon-intensities (2025).
57. Canadian Fuels Association. Clean Fuel Regulations. https://www.canadianfuels.ca/industry-facts/low-carbon-fuels/clean-fuel-regulations (2025).
58. Government of Canada. Clean Fuel Regulations (SOR 2022-140). laws-lois.justice.gc.ca/eng/regulations/SOR-2022-140/page-6.html#h-1359334 (2022).
59. European Commission Joint Research Centre. Renewable Energy - Recast to 2030 (RED II). https://joint-research-centre.ec.europa.eu/welcome-jec-website/reference-regulatory-framework/renewable-energy-recast-2030-red-ii_en (2025).
60. Ahlgren, S. & Di Lucia, L. Indirect land use changes of biofuel production–a review of modelling efforts and policy developments in the European Union. *Biotechnol. Biofuels* **7**, 35 (2014).
61. Lee, H. et al. IPCC, 2023: Climate change 2023: Synthesis report, summary for policymakers. Contribution of working groups i, II and III to the sixth assessment report of the intergovernmental panel on climate change [core writing team, H. Lee and J. Romero (Eds.)]. IPCC, Geneva, Switzerland. (2023).
62. Ecoinvent. ecoinvent cutoff system model, version 3.8. https://ecoquery.ecoinvent.org/3.8/cutoff (2025).
63. Argonne National Laboratory. GREET model. https://greet.anl.gov/ (2025).
64. Yoel et al. Bio-based Oxalic Acid Production in Issatchenkia orientalis Enables Sustainable Rare Earth Recovery. *BioSTEAMDevelopmentGroup/Bioindustrial-Park: Jan2026*, https://doi.org/10.5281/zenodo.18234694 (2026).

Acknowledgements

This work was funded by the DARPA Environmental Microbes as a Bioengineering Resource (EMBER) program (contract DE-AC52-07NA27344) (R.H., Y.J., and H.Z.). Distribution Statement A. Approved for public release: distribution is unlimited. The views, opinions, and/or findings expressed are those of the authors and should not be interpreted as representing the official views or policies of the Department of Defense or the U.S. Government. Work at LLNL was performed under the auspices of the U.S. Department of Energy by Lawrence Livermore National Laboratory under Contract DEAC52-07NA27344 (LLNL-JRNL-2014570). The online tool BioRender (biorender.com) was used to create Fig. 1 and Fig. 2a. We thank Vinh G. Tran from University of Illinois Urbana-Champaign for discussion about the metabolic engineering design, Keith D. Morrison from Lawrence Livermore National Laboratory for his assistance with X-ray diffraction data collection, and Forrest Dills form University of Kentucky for his assistance for precipitation test.

Author contributions

J.L. and H.Z. conceived and designed the study. J.L. performed all experiments related to the metabolic engineering and fermentation. Z.D., Y.J. and D.P. performed the precipitation test, structural and chemical analyses via X-ray diffraction and Fourier transform infrared spectroscopy. A.J. and R.H. performed the precipitation test using the allanite leachate as substrate. W.G. and S.B. performed biomanufacturing facility design, modeling, techno-economic analysis, and life cycle assessment. S.T. and Z.Z. assisted with the construction of plasmids. J.L., W.G., Z.D., S.B., J.G. and H.Z. wrote the manuscript with input from all other authors.

Competing interests

The authors declared no competing interests.

Additional information

Supplementary information The online version contains supplementary material available at https://doi.org/10.1038/s41467-026-68957-5.

Correspondence and requests for materials should be addressed to Huimin Zhao.

Peer review information *Nature Communications* thanks Baskar Gurunathan, and the other, anonymous, reviewer(s) for their contribution to the peer review of this work. A peer review file is available.